Proc. Natl. Acad. Sci. USA
Vol. 96, pp. 4908–4913, April 1999
Biophysics

Motility of ActA protein-coated microspheres driven by actin polymerization

LISA A. CAMERON*, MATTHEW J. FOOTER†, ALEXANDER VAN OUDENAARDEN‡, AND JULIE A. THERIOT†§¶

*Department of Biological Sciences, Stanford University, Stanford, CA 94305-5020; †Department of Biochemistry, Stanford University School of Medicine, Stanford, CA 94305-5307; ‡Department of Chemistry, Stanford University, Stanford, CA 94305-5080; and §Department of Microbiology and Immunology, Stanford University School of Medicine, Stanford, CA 94305-5124

Communicated by James A. Spudich, Stanford University School of Medicine, Stanford, CA, March 1, 1999 (received for review January 12, 1999)

ABSTRACT **Actin polymerization is required for the generation of motile force at the leading edge of both lamellipodia and filopodia and also at the surface of motile intracellular bacterial pathogens such as *Listeria monocytogenes*. Local catalysis of actin filament polymerization is accomplished in *L. monocytogenes* by the bacterial protein ActA. Polystyrene beads coated with purified ActA protein can undergo directional movement in an actin-rich cytoplasmic extract. Thus, the actin polymerization-based motility generated by ActA can be used to move nonbiological cargo, as has been demonstrated for classical motor molecules such as kinesin and myosin. Initiation of unidirectional movement of a symmetrically coated particle is a function of bead size and surface protein density. Small beads (≤0.5 μm in diameter) initiate actin-based motility when local asymmetries are built up by random fluctuations of actin filament density or by thermal motion, demonstrating the inherent ability of the dynamic actin cytoskeleton to spontaneously self-organize into a polar structure capable of generating unidirectional force. Larger beads (up to 2 μm in diameter) can initiate movement only if surface asymmetry is introduced by coating the beads on one hemisphere. This explains why the relatively large *L. monocytogenes* requires polar distribution of ActA on its surface to move.**

Listeria monocytogenes is a Gram-positive intracellular bacterial pathogen that moves rapidly through host cells or cytoplasmic extracts, propelled by actin hijacked from the host cell (1–3). Moving bacteria are associated with an actin-rich structure that resembles the tail of a comet (4). The actin filaments within the comet tail remain fixed in space as the bacterium moves, and the rate of bacterial movement is tightly correlated with the rate of actin filament polymerization at the front of the comet tail (5, 6). Because no motor proteins have been found to be involved in this form of motility, filament elongation is thought to provide the force necessary to propel the bacterium through the cytoplasm (7). The comet tail structure is functionally similar to the actin meshwork in the lamellipodia of a locomoting eukaryotic cell, and the surface of the bacterium is analogous to the leading edge. Therefore, insights into the mechanism of actin-based bacterial movement should help explain the mechanisms of eukaryotic actin-based motility.

A bacterial comet tail is made up of short (0.2–0.3 μm) actin filaments crosslinked together to form a dense cylindrical structure (4). Other intracytoplasmic pathogens form similar comet tail structures and undergo actin-based motility, including the unrelated bacteria *Shigella flexneri* (8) and *Rickettsia* spp. (9) and vaccina virus (10). In uninfected cells and cytoplasmic extracts, actin-rich comet tails are associated with moving endosomes (J. Heuser, personal communication) and phospholipid vesicles (11). Although much is understood about the biochemical mechanisms of catalyzing actin filament polymerization in several of these systems (12–14), relatively little is known about how this local surface catalysis results in comet tail formation, force generation, and motility. It is striking that a variety of biochemical mechanisms for catalyzing local actin polymerization on the surface of a small object (bacterium, virus, or membrane vesicle) all result in the same type of actin self-organization and movement.

A single *L. monocytogenes* gene product, ActA, has been identified as being important for actin-based motility. ActA is distributed on the bacterial surface in a polar fashion, and the pole with the higher ActA density is associated with the comet tail (15). Mutant strains deficient in expression of this protein cannot associate with actin or move intracellularly (16–18). Expression of ActA in the nonpathogenic *Listeria innocua* (19) or asymmetric attachment of purified protein to the cell wall of *Streptococcus pneumoniae* (20) confers actin-based motility on those heterologous organisms. To shed light on the role of asymmetry of ActA distribution and the mechanism by which local actin polymerization translates into force generation, we have created a simplified system in which parameters governing movement initiation can be varied easily.

MATERIALS AND METHODS

Protein Purification and Bead Coating. ActA-His was purified from strain DP-L2723 of *L. monocytogenes* (a gift from Daniel Portnoy, University of California, Berkeley) expressing a truncated *actA* gene encoding amino acids 1–613 described in ref. 14. A flask containing 50 ml of brain heart infusion media with 10 μg/ml chloramphenicol was inoculated with one colony of DP-L2723 and was grown overnight (8 hr) at 37°C. The bacterial culture was divided between 2 × 1 liter of modified D10 minimal media (originally reported in ref. 21 with amino acid supplements of 1.55 mM L-glutamine, 1.74 mM L-asparagine, 1.94 mM L-cysteine, and 1.77 mM L-leucine, 150 μM EDTA in lieu of nitrilotriacetic acid, 180 μM $FeN_3O_9{\cdot}9H_2O$ for the iron source, and glucose added to 0.4%) with 20 μg/ml chloramphenicol and was grown for 12–18 hr at 37°C in the dark. After bacteria were pelleted, 2 g of DE52 resin (Whatman) was added to supernatant containing secreted protein and was incubated for 1 hr with agitation. All subsequent steps were performed at 4°C. The resin was collected by centrifugation and was washed free of D10 media with 20 mM Tris (pH 7.9) and 100 mM NaCl. ActA was eluted in batch from the DE52 resin with 15 ml of 20 mM Tris (pH 7.9) and 500 mM NaCl. Eluate was diluted to 20 mM Tris (pH 7.9) and 250 mM NaCl (buffer A) and was loaded onto a 5-ml nickel nitrilotriacetic acid agarose (Qiagen, Valencia, CA)

The publication costs of this article were defrayed in part by page charge payment. This article must therefore be hereby marked "*advertisement*" in accordance with 18 U.S.C. §1734 solely to indicate this fact.

PNAS is available online at www.pnas.org.

¶To whom reprint requests should be addressed at: Department of Biochemistry, Stanford University School of Medicine, 300 Pasteur Drive, Stanford, CA 94305-5307. e-mail: theriot@cmgm.stanford.edu.

column. The column was washed with buffer A and was developed with a linear gradient of buffer B (20 mM Tris, pH 7.9/500 mM NaCl/1 M Imidazole). ActA-His came off the column at 250 mM Imidazole. Protein was further purified on a HiTrap Q (Amersham Pharmacia) column by using a gradient of NaCl from 20 mM to 1 M in 20 mM Bis-Tris (pH 6.5). ActA-His eluted at 250 mM NaCl and was stored at −80°C.

Carboxylated polystyrene beads (Polysciences), ranging in size from 0.2 μm to 0.9 μm, were incubated in protein solution containing the stated percentage of ActA-His and supplemented with ovalbumin to 2 mg/ml final protein concentration. In all cases, conditions were such that the amount of protein was saturating. For example, 2 μl of 0.5-μm beads (2.5% solids) were added to 10 μl of protein solution; volume was adjusted to account for changes in surface area when beads of different sizes were used. Beads were incubated in protein solution for 1 hr at room temperature and then were pelleted and washed in XB (100 mM KCl/0.1 mM $CaCl_2$/2 mM $MgCl_2$/5 mM EGTA/10 mM K·Hepes, pH 7.7) and were resuspended in 30 μl of XB. Protein-coated beads were stored on ice or at 4°C and were used for up to 1 week.

Asymmetric Beads. To introduce asymmetry on beads, 5 μl of beads (0.025% latex solids in ethanol) were dried onto 22-mm-square coverslips. The coated coverslips were placed into a vacuum evaporator and were shadowed at an angle of 3–4° by using silicon monoxide in a tungsten basket at 10^{-5} torr (1 torr = 133 Pa). To confirm asymmetry, the shadowed beads, on coverslips, were treated with 10% aminopropyltriethoxysilane in dimethylformamide for 30 minutes (to reduce the background staining visible on the bare glass in the shadow of the bead), were rinsed in water, and were incubated in 0.08 mg/ml rhodamine-BSA. For labeling with ActA-His, beads were removed from the coverslip by using a microspatula and were treated as described for the symmetric beads. Micrographs were taken as described below.

Motility Assays. For visualizing bead motility, ActA-His-coated beads (0.5 μl) were added to *Xenopus laevis* egg cytoplasmic extract (7 μl) (prepared as described in ref. 2) supplemented with tetramethylrhodamine iodoacetamide-labeled actin (1.5 μl of 4.5 mg/ml rhodamine-actin in 50 μl) (prepared as described ref. 22) and ATP regenerating mix (23). The assay mix was allowed to incubate on ice for 1 hr. Then, a 1.2-μl sample was removed and was squashed between a microscope slide and 22-mm-square glass coverslip, was sealed with vaseline:lanolin:paraffin (at 1:1:1), and was incubated at room temperature for 1 hr in the dark before observing on the microscope. All observations were performed on a Nikon Diaphot-300 inverted microscope equipped with phase contrast and epifluorescence optics. Time-lapse video microscopy was achieved with an intensified charge-coupled device camera [Dage–MTI (Michigan City, IN) GenIISys/CCD-c72] by using METAMORPH (Universal Imaging, Media, PA) software. Phase contrast/fluorescence image pairs were recorded every 10 sec, with eight video frames averaged per image. Rates of movement were determined by averaging the distance moved in 100 sec in 10 adjacent time intervals. For the measurement of fraction of beads with tails and intensity of bead fluorescence, single phase contrast/fluorescent image pairs of several fields were captured for quantification.

RESULTS

Carboxylated polystyrene beads were coated with a purified form of ActA in which the transmembrane domain has been replaced by 6× His (ActA-His). Surprisingly, when added to *Xenopus* egg extracts containing rhodamine-actin, ActA-His-coated beads with a diameter of 0.5 μm moved at rates comparable to *L. monocytogenes*, seemingly without the need for asymmetric protein distribution. Initially, beads formed symmetric, brightly fluorescent actin clouds. Within 1 hr, a subset of the beads began to move, generating comet tails similar in shape and dynamic behavior to those seen in *L. monocytogenes* motility (Fig. 1). This result demonstrates that comet tail formation and actin-based motility require neither bacterial factors other than ActA nor, apparently, asymmetric surface distribution of ActA.

This *in vitro* assay permits us to vary parameters that cannot be easily manipulated in living bacteria, including protein surface density and particle size. By varying these parameters, we can begin to understand how asymmetric movement is initiated by a symmetrically coated bead. The number of motile beads associated with tails strongly depended on the density of ActA-His on the surface (Fig. 2*a*) and was highest at a surface density of 37.5% ActA-His. Protein surface density of ActA was varied by mixing ActA-His with ovalbumin at various ratios because ovalbumin and ActA-His adsorbed about equally well to the carboxylated latex particles (data not shown). Even though surface protein density affected the fraction of beads with tails, the velocity of a bead once it started moving was independent of ActA-His density (Fig. 2*b*). Over an ActA-His surface density range of 25–100%, 0.5-μm beads moved at a rate of 0.119 ± 0.023 μm/sec (n = 56), similar to the velocity of *L. monocytogenes* in the same cytoplasmic extract (0.126 ± 0.035 μm/sec, n = 23).

Stationary beads exhibited a wide range of cloud densities, at every protein concentration. Overall, beads with higher surface densities of ActA-His tended to form clouds with a greater actin content, but this dependence was not linear with ActA-His surface density (Fig. 2*c*). This observation indicates that assembly of actin clouds is a complex, cooperative process that is not simply determined by the local concentration of ActA-His. Samples coated with the lowest densities of ActA-His showed the greatest variability in actin cloud density, with some very brightly fluorescent clouds and some that were not discernable above background (note SD in Fig. 2*c*). Beads coated with the highest densities of ActA-His exhibited more

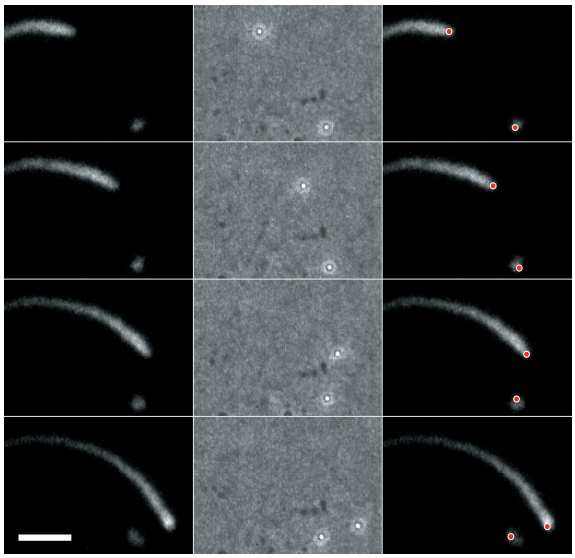

FIG. 1. Actin-based movement of a 0.5-μm-diameter carboxylated polystyrene microsphere uniformly coated with ActA-His. ActA-His-coated microspheres were incubated in *Xenopus* egg cytoplasmic extract supplemented with 0.15 mg/ml rhodamine-actin. Four frames from a video sequence are shown, each separated by 30 sec. A stationary bead surrounded by an actin cloud is at the lower right. (Left column) Fluorescence image showing distribution of rhodamine-actin in the comet tail and cloud. (Center column) Phase-contrast image showing position of polystyrene beads. (Right column) Bead positions (red dots) superimposed on fluorescence images. This bead is moving at a rate of 0.153 μm/sec. (Bar = 5 μm.)

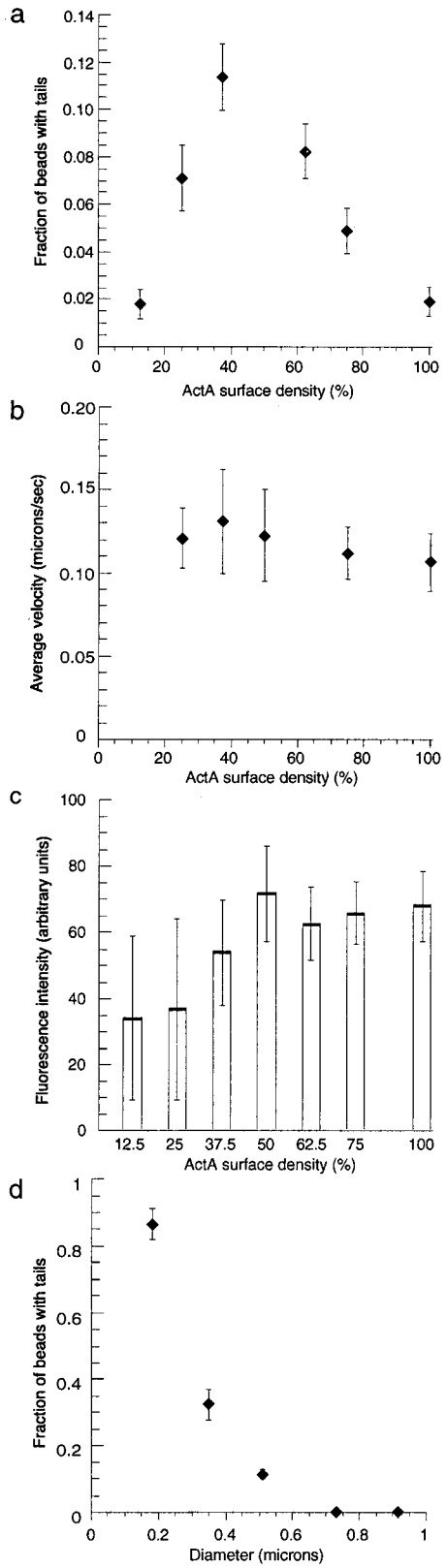

FIG. 2. Motility depends on ActA-His surface density and particle size. (*a*) For 0.5-μm-diameter polystyrene beads, the probability of comet tail formation strongly depended on ActA-His surface density. Initiation of movement was most efficient when ≈37.5% of available sites were occupied by ActA-His; higher and lower densities inhibited tail formation. Error bars are ±SD. Between 380 and 630 beads were scored at each surface density. (*b*) For moving 0.5-μm-diameter polystyrene beads, average velocity was independent of ActA-His surface density. Error bars are ±SD; n = 8–16 beads for each point. Differences between points are not statistically significant by Student's t test. Average velocity of *L. monocytogenes* in this extract was 0.126 ± 0.035 μm/sec; n = 23. (*c*) For nonmoving 0.5-μm-diameter polystyrene beads, the intensity and variability of the actin clouds depended on ActA-His surface density. Error bars are ±SD; n = 57–125 for each concentration. Note that SD is large for low ActA surface densities and decreases substantially at higher densities. (*d*) At optimal ActA-His surface density (37.5% of available sites), the probability of comet tail formation strongly depended on bead diameter. Beads with diameters of 0.7 μm or greater were never observed to form tails whereas most beads of 0.2-μm-diameter formed tails. Error bars are ±SD; n = 100–600 per point. All results (*a–d*) were taken at a 1-hr time-point of incubation at room temperature.

uniformly bright clouds. Because these beads also were less likely to move than those coated with an intermediate amount of ActA-His, we conclude that dense, uniform actin filament accumulation inhibits the initiation of movement.

The likelihood of movement also depends on the size of the bead. ActA-coated beads 0.5 μm in diameter or smaller (0.2 and 0.35 μm) generated comet tails; however, 0.7- or 0.9-μm beads did not (Fig. 2*d*). After 1 hr of incubation at room temperature, >80% of 0.2-μm beads had tails, but this percentage fell off sharply with increasing size, to 12% at 0.5 μm. This very strong size-dependence suggests that random thermal motions of the beads may be involved in the initiation of movement. Interestingly, the rate of movement decreased with size; 0.35-μm beads had an average velocity of 0.0609 ± 0.0130 μm/sec (n = 38), and 0.2-μm beads moved at 0.0497 ± 0.0129 μm/sec (n = 46).

Two models may explain the transition of a uniform cloud to a polar structure: random bead movement as a result of thermal motion or local variations in filament density and in cross-linking of actin filaments in the cloud surrounding the bead. The strong size-dependence we have observed is more consistent with the former mechanism, but our observation that actin cloud assembly is highly cooperative and nonlinear lends credence to the latter. To separate the relative contributions of these two sources of asymmetry, we tracked movements of 0.5-μm-diameter beads within actin clouds immediately before comet tail formation (Fig. 3*a*). Small random movements reminiscent of thermal motion were apparent, but rapid, directed movement occurred only after a buildup of asymmetric actin density in the cloud (Fig. 3 *b–f*). This individual bead made multiple escape attempts in different directions sequentially. A failed escape attempt was followed by a recovery of cloud symmetry, followed by a new focal actin accumulation at another, seemingly random, location within the cloud. When the bead escaped from the cloud, it was immediately moving at its maximum velocity, which is expected for an object with negligible inertia. We suspect that slow accumulations of asymmetric dense actin foci are mediated by actin crosslinking proteins, which are required for comet tail formation (24). Fig. 3 shows a representative experiment. Movement initiation was recorded for 12 beads in which a total of 35 velocity spikes on the order of 0.1 μm/sec were observed. All of the velocity spikes correlated with a large asymmetry value from 0.5 to 1.0.

Because a single bead can move sequentially in different directions (Fig. 3*a*), and because a single cloud can gain and lose asymmetry over time (Fig. 3*e*) and may have two or more local zones of high actin density simultaneously (Fig. 3*d*, note, particularly, 1,100–1,200 sec), we conclude that the actin density variations we observed are due to stochastic variation in actin filament polymerization and crosslinking dynamics rather than by microheterogeneity in distribution of ActA-His on the bead surface, which would be temporally invariant. Our observations indicate that random local fluctuations in filament density and crosslinking are self-reinforced and can lead to symmetrically coated beads being forced out of the cloud,

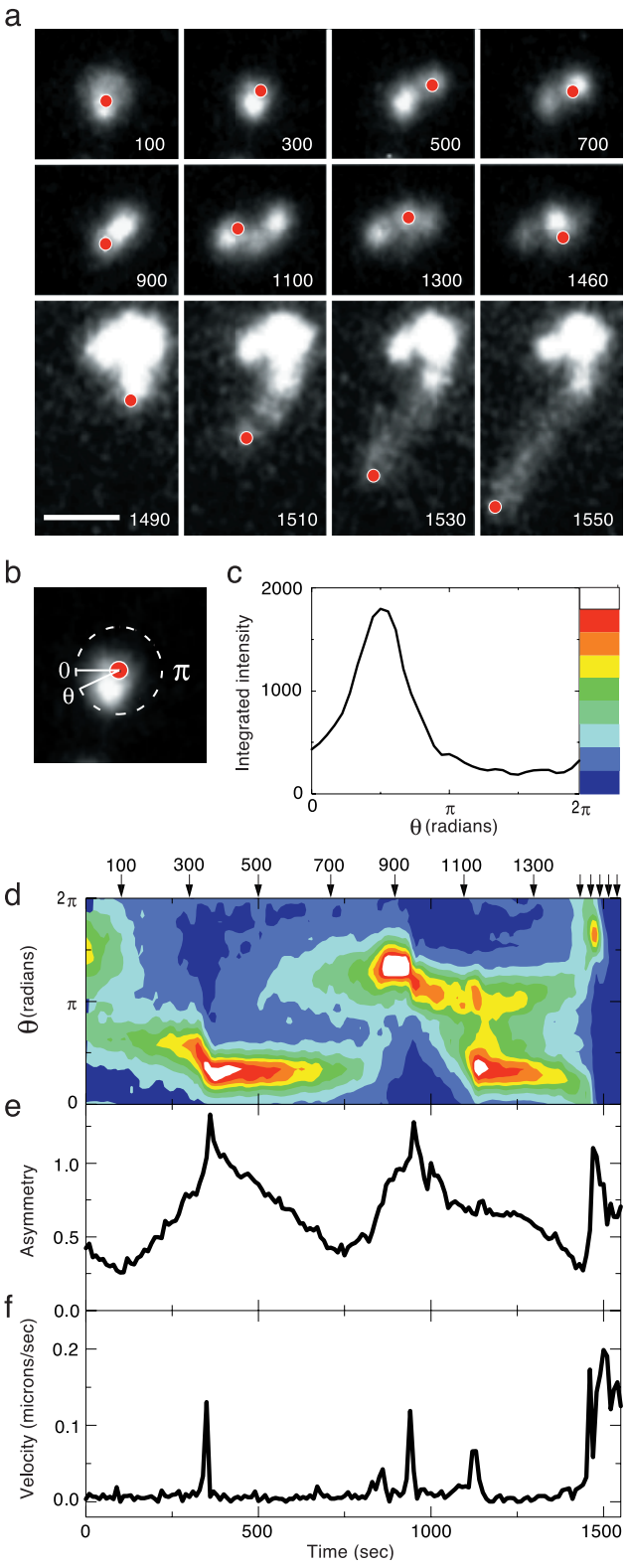

FIG. 3. Asymmetry builds up in the actin cloud before bead takeoff. (*a*) Video sequence of a 0.5-μm-diameter ActA-His-coated bead during the transition from cloud to tail. Rhodamine-actin fluorescence is depicted in gray-scale. The position of the polystyrene bead, as determined from paired phase-contrast images, is indicated by the red dots. Actin filament density in the cloud becomes strikingly asymmetric, and the particle bounces around within the confines of the cloud, before escaping and moving rapidly away ≈1,480 sec into the video sequence. Total time elapsed in seconds is shown at the bottom right corner of each frame. Note time compression for the four frames in the bottom row. The contrast in these last four frames has been digitally enhanced relative to the first eight, so that the dimmer comet tail can be seen as well as the bright cloud. (Bar = 5 μm.) (*b*) Angular variation of actin density within the cloud for one frame from the video sequence shown in *a* (at 300 sec). Fluorescence intensity within a circle of 1-μm radius centered on the bead varies as a function of radial angle θ. (*c*) Actin filament density distribution as a function of angle for the video frame shown in *b*. For each value of the angle θ, the fluorescence intensity is integrated over a wedge-shaped segment between $\theta - \pi/36$ and $\theta + \pi/36$ within a radius of 1 μm around the bead. Color bar shows translation of integrated fluorescence intensity into a color scale, used in *d*. (*d*) Actin filament density distribution around this bead as a function of time. The arrows indicate the frames shown in *a*. Integrated fluorescence intensity as a function of angle was determined as in *c* for each frame in the video sequence and was depicted by using a color scale. This contour plot shows fluorescence intensity in the cloud as a function of both time and angle. Note that there are two distinct peaks of actin density at 1,125 sec. Note also that each of the three peaks in the contour plot correlates with a velocity spike in *f*. This plot does not show the obvious asymmetry after the bead starts moving because the fluorescence intensity of the tail is far below that of the actin cloud. (*e*) Cloud asymmetry for this bead as a function of time. An asymmetric distribution of actin filaments gradually builds in the cloud before each burst of speed. "Asymmetry" here is a scalar describing the degree to which actin filament density is concentrated in a particular sector of a circle centered on the bead. Asymmetry is calculated by computing the SD of the fluorescence intensity as a function of θ and normalizing to the mean values at each time point. A perfectly spherical cloud (SD = 0) would have an asymmetry of 0, but, due to the finite noise in fluorescence intensity, the measured asymmetry is larger. (*f*) Velocity of this bead as a function of time. Superimposed on apparently random thermal motion of the particle are several sharp velocity peaks that correspond to peaks in actin filament density apparent in *d* before the rapid escape of the particle near the end of the sequence.

initiating comet tail formation. Breaking of symmetry is easier for smaller beads, which undergo more thermal motion (Fig. 2*d*), and is more difficult for beads with higher concentrations of ActA-His, where variability in filament density is reduced (Fig. 2 *a* and *c*).

We have demonstrated that symmetric beads are able to initiate movement, so why is asymmetric attachment of ActA to the cell surface required for bacterial movement? In our *in vitro* system, symmetric beads >0.5 μm in diameter did not form tails. The cylindrical *L. monocytogenes* are ≈0.7 μm in diameter and 2 μm long, substantially larger than the threshold for spontaneous asymmetry. To test the hypothesis that surface asymmetry can allow movement initiation for larger beads, we coated carboxylated polystyrene microspheres on one hemisphere by using low-angle shadowing. Protein adsorbed preferentially to the uncoated polystyrene surface (Fig. 4 *a* and *b*). This artificial asymmetry had three effects on ActA-His-induced bead movement. First, it increased the likelihood that 0.5-μm beads would form comet tails and move, from 12% if symmetrically coated to 50% if asymmetrically coated. Second, asymmetry conferred motility on beads that were too large to move when symmetrically coated with ActA-His. Shadowed beads with a diameter of 1 μm moved at rates of ≈0.10 μm/sec (Fig. 4*c*), similar to the velocity of *L. monocytogenes* or symmetrically coated smaller beads, and even 2-μm beads moved, although less frequently and at slower rates (Fig. 4*d*). Third, asymmetric beads moved when the ActA-His surface density was as low as 5%, less than half that of the 12.5% required for symmetrically coated particles.

DISCUSSION

We have shown that ActA-coated polystyrene beads will form actin-rich comet tails and move in cytoplasmic extract without any other components of the bacterial cell surface. This demonstrates that an actin polymerization-dependent motor can move artificial cargo, as has been shown for classical

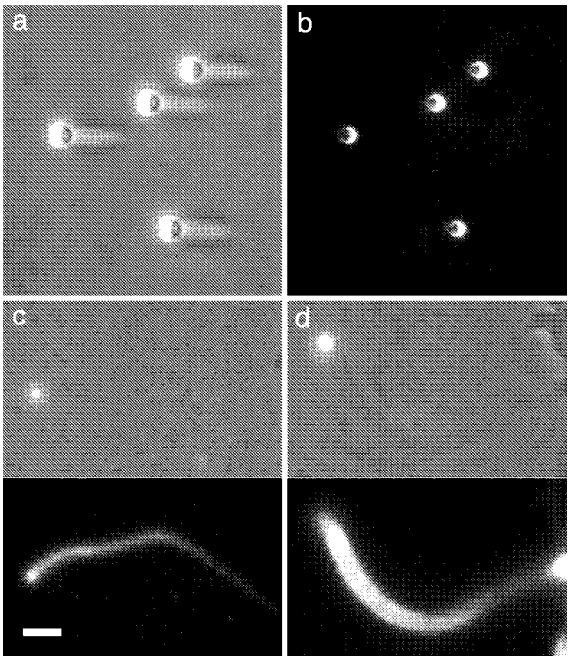

FIG. 4. Movement of larger beads asymmetrically coated with ActA-His. (*a*) 2-μm-diameter carboxylated polystyrene beads shadowed from the left with silicon monoxide. Shadows can be seen on the protected side of the beads in this phase-contrast image. (Bar = 5 μm.) (*b*) Shadowed beads shown in *a* were incubated *in situ* with rhodamine-conjugated BSA and were washed and imaged using epifluorescence. Labeled protein adsorbed preferentially to the uncoated polystyrene surface. (*c*) Comet tail formation by a 1-μm-diameter shadowed carboxylated polystyrene bead, coated asymmetrically with ActA-His at 12.5% of available sites. (*Upper*) Phase-contrast. (*Lower*) Rhodamine-actin fluorescence. This bead is moving at a rate of 0.088 μm/sec. (*d*) 2-μm-diameter bead treated as in *c* moving at a rate of 0.019 μm/sec.

molecular motors such as myosin and kinesin (25, 26). 0.5-μm beads move at rates comparable to *L. monocytogenes* in cell extracts, regardless of the protein surface density on the bead. However, smaller beads (which are more likely to form tails) move at slower rates. One proposed "Brownian rachet" mechanism for actin polymerization-driven movement requires that the object being moved (in this case, the bead) diffuse far enough from the tip of the elongating actin filament to allow intercalation of a new actin monomer (27). In this model, smaller beads are predicted to move faster, with velocity proportional to the diffusion coefficient. Our results rule out this model. However, other Brownian rachet models in which the actin filaments themselves undergo thermal fluctuations are still viable (7).

ActA-dependent movement requires the establishment of an asymmetric distribution of actin filaments on or near the bead surface. Asymmetry may arise from either self-reinforced fluctuations in actin filament density and crosslinking, which can be exaggerated by thermal motion, or by surface asymmetry of the particle. If asymmetry is introduced by shadowing of the beads, larger objects are able to move, and lower ActA surface densities will support initiation of movement. This suggests that bacteria must distribute ActA asymmetrically on the cell surface because their size is relatively large. For smaller objects that use actin comet tails to move, such as vaccinia virus (10) and lipid vesicles (11), our observations suggest that symmetry may be broken spontaneously. In contrast to bacteria, there is no clear mechanism by which viruses or vesicles could establish stable surface asymmetry, so the self-reinforced spontaneous symmetry breaking we have observed provides a satisfying explanation for their ability to initiate unidirectional movement.

The simplified system we describe here represents important general features of cytoskeletal self-organization and actin-based motility. Local application of a chemotactic agent near the surface of a motile eukaryotic cell can result in local actin polymerization, extension of lamellipodia, cell polarization, and directed movement of the cell toward the chemotactic agent. Remarkably, motile eukaryotic cells exposed to a uniform concentration of a chemotactic agent will spontaneously develop cytoskeletal polarity and will initiate rapid movement in a persistent, random walk, even though they have no signal gradient to move up (28). Our results suggest that this spontaneous self-organization and inclination toward polarity is an inherent property of actin cytoskeletal dynamics. Local protrusive or propulsive force due to accumulation of polymerized actin is a cooperative response that is highly dependent on filament crosslinking and other factors.

Our *in vitro* system recapitulates this important general feature of actin self-organization in a highly simplified manner. Asymmetry is required for directional motility and may develop from local variation in density of nucleation sites, random fluctuations in local filament density, thermal fluctuations in the position of the nucleating structure, or a combination of all three. Because of the nonlinearity and positive feedback mechanisms built into the cytoskeleton, any source of asymmetry can be amplified and reinforced to allow initiation of unidirectional movement. The dynamic actin cytoskeleton is poised to push and will jump at any excuse to do so.

We gratefully acknowledge Gregory Smith and Daniel Portnoy for the gift of *L. monocytogenes* strain DP-L2723 for generating ActA-His, Peter Jackson and Tim Stearns for providing *X. laevis* to make egg extract, and Eugene Smith (Research Devices, Inc., Sunnyvale, CA) for assistance with low-angle shadowing. We thank Kevin Lustig, Sandra McCallum, Jennifer Robbins, and George Somero for critical comments on the manuscript. This work was supported by National Institutes of Health Grant RO1 AI36929 to J.A.T. A.v.O. acknowledges financial support from the Dutch Organization for Scientific Research (NWO).

1. Dabiri, G. A., Sanger, J. M., Portnoy, D. A. & Southwick, F. S. (1990) *Proc. Natl. Acad. Sci. USA* **87,** 6068–6072.
2. Theriot, J. A., Rosenblatt, J., Portnoy, D. A., Goldschmidt-Clermont, P. J. & Mitchison, T. J. (1994) *Cell* **76,** 505–517.
3. Welch, M. D., Iwamatsu, A. & Mitchison, T. J. (1997) *Nature (London)* **385,** 265–269.
4. Tilney, L. G. & Portnoy, D. A. (1989) *J. Cell Biol.* **109,** 1597–1608.
5. Theriot, J. A., Mitchison, T. J., Tilney, L. G. & Portnoy, D. A. (1992) *Nature (London)* **357,** 257–260.
6. Sanger, J. M., Sanger, J. W. & Southwick, F. S. (1992) *Infect. Immun.* **60,** 3609–3619.
7. Mogilner, A. & Oster, G. (1996) *Biophys. J.* **71,** 3030–3045.
8. Bernardini, M. L., Mounier, J., d'Hauteville, H., Coquis-Rondon, M. & Sansonetti, P. J. (1989) *Proc. Natl. Acad. Sci. USA* **86,** 3867–3871.
9. Heinzen, R. A., Hayes, S. F., Peacock, M. G. & Hackstadt, T. (1993) *Infect. Immun.* **61,** 1926–1935.
10. Cudmore, S., Cossart, P., Griffiths, G. & Way, M. (1995) *Nature (London)* **378,** 636–638.
11. Ma, L., Cantley, L. C., Janmey, P. A. & Kirschner, M. W. (1998) *J. Cell Biol.* **140,** 1125–1136.
12. Carlier, M. F., Laurent, V., Santolini, J., Melki, R., Didry, D., Xia, G. X., Hong, Y., Chua, N. H. & Pantaloni, D. (1997) *J. Cell Biol.* **136,** 1307–1323.
13. Suzuki, T., Miki, H., Takenawa, T. & Sasakawa, C. (1998) *EMBO J.* **17,** 2767–2776.
14. Welch, M. D., Rosenblatt, J., Skoble, J., Portnoy, D. A. & Mitchison, T. J. (1998) *Science* **281,** 105–108.
15. Kocks, C., Hellio, R., Gounon, P., Ohayon, H. & Cossart, P. (1993) *J. Cell Sci.* **105,** 699–710.
16. Kocks, C., Gouin, E., Tabouret, M., Berche, P., Ohayon, H. & Cossart, P. (1992) *Cell* **68,** 521–531.
17. Domann, E., Wehland, J., Rohde, M., Pistor, S., Hartl, M., Goebel, W., Leimeister-Wachter, M., Wuenscher, M. & Chakraborty, T. (1992) *EMBO J.* **11,** 1981–1990.

18. Brundage, R. A., Smith, G. A., Camilli, A., Theriot, J. A. & Portnoy, D. A. (1993) *Proc. Natl. Acad. Sci. USA* **90,** 11890–11894.
19. Kocks, C., Marchand, J. B., Gouin, E., d'Hauteville, H., Sansonetti, P. J., Carlier, M. F. & Cossart, P. (1995) *Mol. Microbiol.* **18,** 413–423.
20. Smith, G. A., Portnoy, D. A. & Theriot, J. A. (1995) *Mol. Microbiol.* **17,** 945–951.
21. Trivett, T. L. & Meyer, E. A. (1971) *J. Bacteriol.* **107,** 770–779.
22. Theriot, J. A. & Fung, D. C. (1998) *Methods Enzymol.* **298,** 114–122.
23. Murray, A. W. (1991) *Methods Cell Biol.* **36,** 581–605.
24. Dold, F. G., Sanger, J. M. & Sanger, J. W. (1994) *Cell Motil. Cytoskeleton* **28,** 97–107.
25. Spudich, J. A., Kron, S. J. & Sheetz, M. P. (1985) *Nature (London)* **315,** 584–586.
26. Vale, R. D., Reese, T. S. & Sheetz, M. P. (1985) *Cell* **42,** 39–50.
27. Peskin, C. S., Odell, G. M. & Oster, G. F. (1993) *Biophys. J.* **65,** 316–324.
28. Coates, T. D., Watts, R. G., Hartman, R. & Howard, T. H. (1992) *J. Cell Biol.* **117,** 765–774.